ISSN 2032-6653

A New Sensorless Drive Control System for Transmissionless EVs Using a Permanent-Magnet Synchronous Motor

Shinji Shinnaka* and Shigeru Takeuchi*

One of the most important technologies for electric vehicles (EVs) will be drive control technology for main traction motors. It is desired for the drive control system to have the following characteristics: 1) it is based on vector control methods that allow quick, efficient and/or precise torque production; 2) it can produce 150-250% rated torque at standstill and can have wide driving-range, consequently can allow development of EVs with no variable-transmission; 3) it does not require a position/speed sensor for controlling motor drive, which has been mounted on a rotor shaft. This paper proposes a new sensorless drive control system for such EVs using a permanent-magnet synchronous motor as a main traction motor. Potential usefulness of the proposed drive control system is examined through the development of a prototype EV capable of driving on public road.

Keywords: electrical drive, controller and control system, synchronous motor, sensorless, transmissionless.

1. INTRODUCTION

One of the most important technologies for electric vehicles (EVs) will be a drive control technology for main traction motors. As traction motors of EVs, ac motors such as induction motor (IM), permanent-magnet synchronous motor (PMSM) are usually employed. It is desired for a drive control system to have the following characteristics:

1) It does not require a position/speed sensor for controlling motor drive, which has been mounted on a rotor shaft.
2) It is based on vector control methods that allow quick, efficient and/or precise torque production.
3) It can produce 150-250% rated torque at standstill and can have wide driving-range, consequently can allow development of EVs with no variable-transmission.

Most of conventional vector control methods can allow the drive control system to have characteristics 2) and 3), but they require a position/speed sensor to be mounted on a rotor shaft for them. Realization of characteristic 1) allows to have some benefits such as increasing of drive control system reliability, increasing mechanical design flexibility, decreasing motor size in direction of shaft, elimination of wiring sensor cable, decreasing a variety of cost related to the sensor etc. Compared with the motor itself, the position/speed sensor is less reliable from electric, mechanical and thermal viewpoints. Dependence on the sensor results in decrease of total reliability of driving control systems, which will be the most important factor of human-ride vehicles. In addition to improvement in system reliability and mechanical design flexibility, cost and size reductions are attractive in EVs where the storage space is often very restricted.

Due to the attractive features of sensorless drive, developments of sensorless-vector-controlled EVs with no variable transmission (in the following, refereed to as sensorless and transmissionless EVs or shortly to as ST-EVs) have been tried so far [1]-[5]. For ST-EVs using an IM, a successful development allowed to drive on public roads in 2001 by Shinnaka et al. was reported [2]. For ST-EVs using a PMSM, such a successful development seems not to be reported so far, although developments keep going [1]-[5]. Under such circumstances, the authors have succeeded in development of such a ST-EV allowed to drive on public road in 2004.

This paper proposes a new drive control system for ST-EVs using a PMSM in a concretive manner by referring to the newly developed prototype ST-EV and examines its potential usefulness. This paper is organized as follows. Section 2 presents a mathematical model and characteristics of PMSM, which is a direct object to be controlled by vector control methods. The model and characteristics form foundations for establishing the drive control system. Section 3 proposes a new configuration of the drive control system. Section 4 proposes a phase estimator that produces good estimates of phase and speed of the traction PMSM in wide speed-range from standstill to overrated speed instead of a position/speed sensor mounted on a rotor shaft. Section 5 proposes a command generator and a command converter that allow efficient and wide speed-range drive with no variable transmission. Section 6 presents experimental results by both a test-bed setup and the prototyped ST-EV on a chassis dynamometer. Section 7 concludes this paper.

2. MATHEMATICAL MODEL AND CHARCTERISTICS OF EV MOTOR

A mathematical model and characteristics of PMSM, which is a direct object to be controlled by vector control methods, form foundations for establishing the drive control system. Consider the general reference frame where orthogonal $\gamma-\delta$ coordinates rotating at an arbitrary instant angular velocity ω as shown in Fig. 1. Rotating polarity is defined such that the direction from principal axis (γ -axis) to secondary axis (δ-axis) is positive. Note that all of the following 2x1 vector signals related to PMSMs are defined in the general reference frame.

A mathematical model for salient-pole PMSMs

* Dept. of Electrical Engineering, Kanagawa University
3-27-1 Rokkakubashi, Kanagawaku, Yokohama
221-8686 Japan
shinnaka@kanagawa-u.ac.jp

ISSN 2032-6653

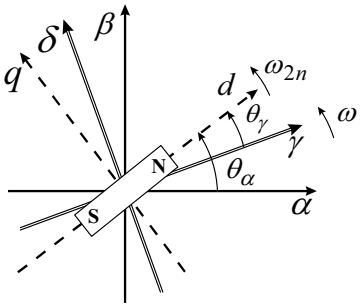

Fig. 1. Phase of rotor N-pole in γ - δ general reference frame rotating at arbitrary angular velocity. ω.

(SP-PMSMs), which consists of three consistent basic equations such as circuit equation, torque evolution equation, and energy transmission, can be described as follows [8], [9]:

Circuit equation (the first basic equation)

$$\boldsymbol{v}_1 = R_1\boldsymbol{i}_1 + \left[s\boldsymbol{I} + \omega\boldsymbol{J}\right]\boldsymbol{\phi}_1 \tag{1}$$

$$\boldsymbol{\phi}_1 = \boldsymbol{\phi}_i + \boldsymbol{\phi}_m \tag{2}$$

$$\boldsymbol{\phi}_i = \left[L_i\boldsymbol{I} + L_m\boldsymbol{Q}(\theta_\gamma)\right]\boldsymbol{i}_1 \tag{3}$$

$$\boldsymbol{\phi}_m = \Phi\boldsymbol{u}(\theta_\gamma) \;\; ; \;\; \Phi = \text{const} \tag{4}$$

$$\boldsymbol{Q}(\theta_\gamma) = \begin{bmatrix} \cos 2\theta_\gamma & \sin 2\theta_\gamma \\ \sin 2\theta_\gamma & -\cos 2\theta_\gamma \end{bmatrix} \tag{5}$$

$$\boldsymbol{u}(\theta_\gamma) = \begin{bmatrix} \cos\theta_\gamma \\ \sin\theta_\gamma \end{bmatrix} \tag{6}$$

$$s\theta_\gamma = \omega_{2n} - \omega \tag{7}$$

Torque evolution equation (the second basic equation)

$$\tau = N_p\left(L_m\boldsymbol{i}_1^T\boldsymbol{J}\boldsymbol{Q}(\theta_\gamma)\boldsymbol{i}_1 + \boldsymbol{i}_1^T\boldsymbol{J}\boldsymbol{\phi}_m\right) \tag{8}$$

Energy transmission equation (the third basic equation)

$$\boldsymbol{i}_i^T\boldsymbol{v}_1 = R_1\|\boldsymbol{i}_1\|^2 + \frac{s}{2}\left(L_i\|\boldsymbol{i}_1\|^2 + L_m\left(\boldsymbol{i}_1^T\boldsymbol{Q}\left(\theta_\gamma\right)\boldsymbol{i}_1\right)\right) + \omega_{2m}\tau \tag{9}$$

where 2x1 vectors $\boldsymbol{v}_1, \boldsymbol{i}_1, \boldsymbol{\phi}_1$ are voltage, current and flux of the stator respectively, 2x1 vectors $\boldsymbol{\phi}_i$, $\boldsymbol{\phi}_m$ are components of the stator flux $\boldsymbol{\phi}_1$, more precisely, $\boldsymbol{\phi}_i$ indicates flux evolved directly by the stator current $\boldsymbol{i}_1$ and $\boldsymbol{\phi}_m$ is flux due to the rotor magnet, $\boldsymbol{I}$ is a 2x2 identity matrix, $\boldsymbol{J}$ is a 2x2 skew symmetric matrix such as

$$\boldsymbol{J} = \begin{bmatrix} 0 & -1 \\ 1 & 0 \end{bmatrix}, \tag{10}$$

τ is the evolved torque, ω_{2n}, ω_{2m} are the electrical and mechanical speeds of the rotor, R_1 is the stator resistance, L_i, L_m is the "in-phase and mirror-phase inductances" having the following relation to the d, q-axes inductances [9]

$$\begin{bmatrix} L_d \\ L_q \end{bmatrix} = \begin{bmatrix} 1 & 1 \\ 1 & -1 \end{bmatrix}\begin{bmatrix} L_i \\ L_m \end{bmatrix}, \tag{11}$$

N_p is the number of pole pairs, and s indicates a differential operator *d/dt*.

Table 1. Characteristics of a SP-PMSM of ST-EV.

R_1	0.0178 (Ω)	rated torque maximum torque	40 (Nm) 100 (Nm)
L_d	0.09 (mH)	rated speed maximum speed	400 (rad/s) 1000 (rad/s)
L_q	0.228 (mH)	rated current maximum current	135 (A, rms) 310 (A, rms)
Φ	0.0335 (Vs/rad)	rated voltage maximum voltage	90 (V, rms) 120 (V, rms)
N_p	4	moment of inertia	0.01275(kgm^2)
rated power maximum power	16(kW) 40(kW)	effective resolution of position sensor	4 x 4096 (p/r)

A SP-PMSM modeled by (1)-(9) is employed as a traction PMSM for the prototype ST-EV, whose characteristics (representative values) are shown in Table 1. One-hour rated output of the traction SP-PMSM is 16-kw, and the maximum output is 40-kw, 250% of one-hour rating. One-hour rating of evolved torque is 40-Nm, and the maximum torque is 100-Nm, 250% of one-hour rating. Rated speed is 400-rad/s in mechanical sense, and the maximum speed is 1000-rad/s, 250% of the rating.

3. BASIC CONFIGURATION OF DRIVE CONTROL SYSTEM FOR ST-EV

Fig. 2 illustrates a basic configuration of the proposed drive control system for ST-EVs. The traction SP-PMSM is coupled to the rear wheels though a differential gear with a constant gear ratio, but no variable transmission. Note that speed ratio between the rotor and the rear wheels is constant in all speed ranges including backward drive. The drive control system features the block circled by a dashed line. The block produces electrical power to be injected to the SP-PMSM according to directions by a d-n-r hand lever and an acceleration foot pedal. The speed meter is driven by speed estimate generated by the drive control system.

The main differences between the ST-EV drive control system and the conventional system are the phase estimator and the high frequency voltage generator (indicated as HFV) for sensorless drive, and the command generator and the command converter for energy-efficient and wide speed-range drive. The following sections explain these components in detail, which are indicated by shaded sub-blocks in Fig. 2.

4. CONFIGURATION OF PHASE ESTIMATOR

4.1 Frequency-hybrid combination

The phase estimator plays a role estimating rotor phase and speed instead of a position/speed sensor, which will be the most important for sensorless drives. It is a matter of common understanding that no single estimation method can appropriately estimate the rotor phase in a wide speed range from zero to overrated speed, and that frequency-hybrid combination of two estimation methods is practical, either of which can operate appropriately in the zero-to-low-speed, or low-to-high-speed range [6], [7].

Fig. 3 roughly shows two typical examples of

ISSN 2032-6653

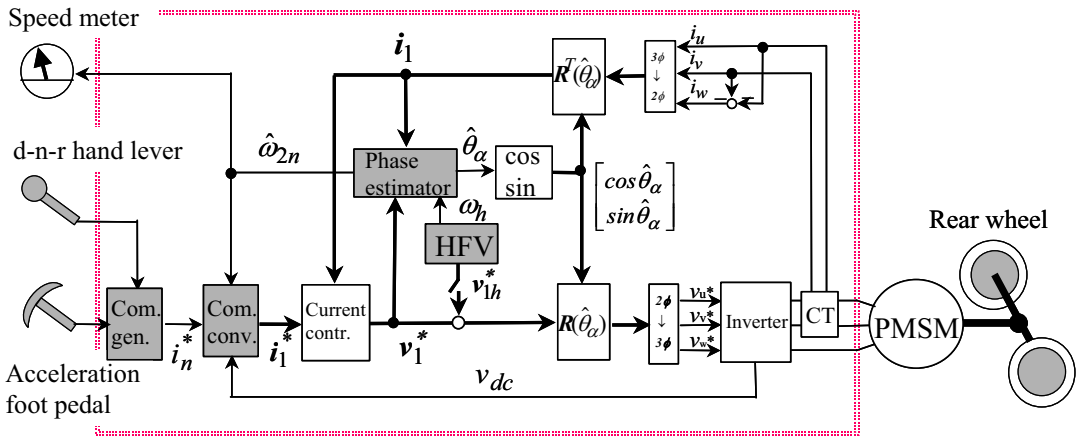

Fig. 2. Basic configuration of drive control system for ST-EVs.

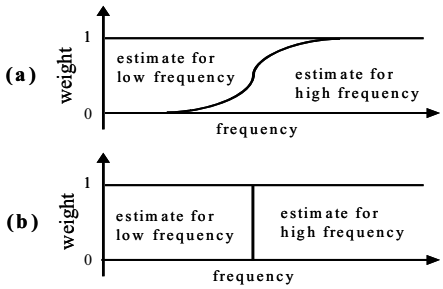

Fig.3. An example of frequency weight for frequency hybrid.

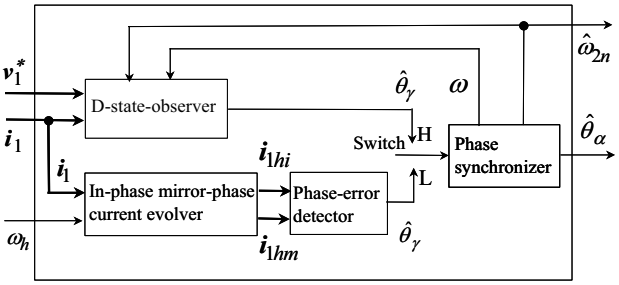

Fig. 4. Configuration of the phase estimator.

frequency-hybrid combination by two phase-estimates produced by different estimation methods. The frequency-dependent weight in (a) varies mildly according to frequency, on the other hand, quickly in (b). The proposed drive control system in Fig. 2 employs type (b) with frequency-dependent weight of unity or zero, and selects weight-changing frequency to be about 600-rad/s in electrical sense for the traction SP-PMSM characterized by Table 1.

Fig. 4 shows a configuration of the phase estimator based on type (b) frequency-hybrid combination with frequency-dependent weight of unity or zero. The phase estimator produces estimates of the rotor phase and speed from inputs of the stator voltage, and current in a rotational reference frame, and the frequency of super-injected high frequency voltage. At electrical frequency about 600-rad/s, the "switch" turns from H-side to L-side or vice versa, one of two the initial phase estimates $\hat{\theta}_\gamma$ is always selected. The phase synchronizer, which plays a role producing the final phase estimate $\hat{\theta}_\alpha$ and the rotor speed estimate, is shared by both phase estimation methods.

4.2 Phase estimation in low-to-high speed range

In low-to-high speed range, for example electrical speed 600~4000-rad/s for the SP-PMSM in Table 1, the rotor phase is estimated using fundamental components of the stator voltage and current, which contributes torque evolution. In the range, the high frequency voltage generator (indicated as HFV) is in principle turned off, and the initial phase estimate $\hat{\theta}_\gamma$ is determined by the "D-state-observer" originally proposed by one of the authors [8]. The D-state-observer has the following attractive characteristics [8].

1) It is a flux-state observer requiring no additional steady-state condition for the dynamic mathematical model of the PMSMs.
2) Its order is the minimum second.
3) Observer gain guaranteeing proper estimation in four quadrants over a wide operating range except singular zero-speed is a simple constant, and can be easily designed (default value is a unity).
4) It utilizes motor parameters in a very simple manner.
5) Its structure is very simple and it can be realized at very low computational load.
6) It can be applied to both of salient pole and non-salient pole PMSMs.
7) The maximum error of steady-state phase estimate can remain within $\pm\pi/4$-rad even if the speed estimate with huge constant error is used in the observer.

The D-state-observer can be described as follows [8]:

D-Sate-Observer

$$\left.\begin{aligned} \boldsymbol{D}(s,\omega)\tilde{\boldsymbol{\phi}}_1 &= \boldsymbol{G}\left[\boldsymbol{v}_1 - R_1\boldsymbol{i}_1\right] + \hat{\omega}_{2n}\left[\boldsymbol{I}-\boldsymbol{G}\right]\boldsymbol{J}\hat{\boldsymbol{\phi}}_m \\ \hat{\boldsymbol{\phi}}_m &= \tilde{\boldsymbol{\phi}}_1 - \boldsymbol{G}\boldsymbol{\phi}_i \end{aligned}\right\} \quad (12)$$

ISSN 2032-6653

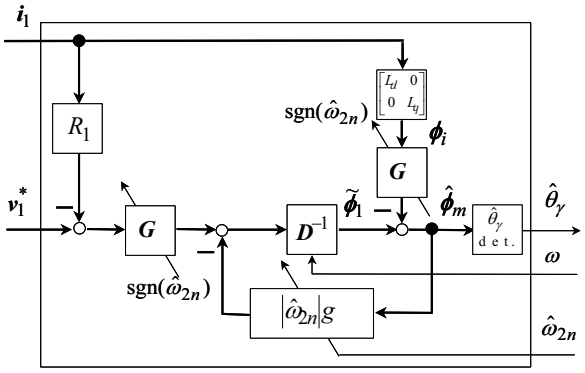

Fig. 5. Configuration of the D-state-observer.

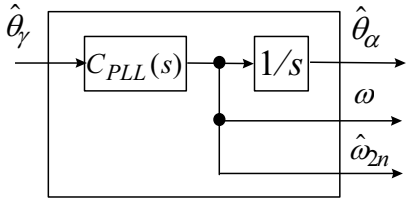

Fig. 6. Configuration of phase synchronizer based on the generalized integral-type PLL method.

$$\left.\begin{aligned}\hat{\boldsymbol{\phi}}_m &= \begin{bmatrix}\hat{\phi}_{md}\\ \hat{\phi}_{mq}\end{bmatrix}\\ \hat{\theta}_\gamma &= \tan^{-1}\frac{\hat{\phi}_{mq}}{\hat{\phi}_{md}} \approx \frac{\hat{\phi}_{mq}}{\Phi}\end{aligned}\right\} \tag{13}$$

with

$$\boldsymbol{D}(s,\omega) = s\boldsymbol{I} + \omega\boldsymbol{J} \tag{14}$$

$$\boldsymbol{\phi}_i \approx \begin{bmatrix}L_d & 0\\ 0 & L_q\end{bmatrix}\boldsymbol{i}_1 \tag{15}$$

$$\boldsymbol{G} = \boldsymbol{I} - \mathrm{sgn}(\hat{\omega}_{2n})g\boldsymbol{J}\ ;\ g = \mathrm{const} > 0\,. \tag{16}$$

Fig. 5 shows the D-state-observer. It is worthy of noting that if the constant observer gain is selected to be zero, i.e. $g = 0$, the D-state-observer results in so-called the "voltage model" in (1)-(4). This fact means that the D-state-observer is the most compact flux-state observer.

The D-state-observer exploits the approximation in (15), which is valid only when the $\gamma - \delta$ coordinates are locked in the d-q coordinates of the rotor reference frame, in other words, only when the convergence property $\hat{\theta}_\gamma \to 0$ holds. The phase lock can be attained by the "generalized integral-type Phase-Locked-Loop (PLL) method," which can be described as follows [9]:

Generalized Integral-Type PLL Method

$$\left.\begin{aligned}\omega &= C_{PLL}(s)\hat{\theta}_\gamma\\ \hat{\omega}_{2n} &= \omega\\ \hat{\theta}_\alpha &= \frac{1}{s}\omega\end{aligned}\right\} \tag{17}$$

with

$$C_{PLL}(s) = \frac{C_n(s)}{C_d(s)} = \frac{c_{nm}s^m + c_{nm-1}s^{m-1} + \cdots + c_{n0}}{s^m + c_{dm-1}s^{m-1} + \cdots + c_{d0}} \tag{18}$$

where polynomials $C_d(s)$, $C_n(s)$ are designed such that the $(m+1)$-th order polynomial defined as in (19) turns out to be a Hurwitz polynomial.

$$H(s) = sC_d(s) + C_n(s) \tag{19}$$

Let $\hat{\theta}_\alpha$ be an estimate of the rotor phase θ_α evaluated in the $\alpha - \beta$ stator reference frame. In a phase-locked state, the convergences $\hat{\theta}_\gamma \to 0$, $\hat{\theta}_\alpha \to \theta_\alpha$ are attained, and the generalized $\gamma - \delta$ reference frame converges to the d-q rotor reference frame. The description using d, q suffixes in (13) is due to this convergence. The phase synchronizer in Fig. 4 is realized according to the generalized integral-type PLL method, as in Fig. 6.

4.3 Phase estimation in zero-to-low speed range

At very low speed, the level of fundamental motor-driving voltage is very small, and its signal-to-noise ratio seriously decreases, furthermore phase estimation based on the fundamental driving signals is in general very sensitive to stator resistance. Consequently, phase estimation using the fundamental motor-driving signals becomes very difficult in the region. In order to cope with the difficulty, the proposed drive control system employs the "mirror-phase estimation method," which was originally proposed by one of the authors [9]. It is a kind of high frequency voltage injection methods and has the following attractive high performance and features.

1) It is directly based on a principle called as the "mirror-phase characteristics", which were recently found to be inherent in ac motors with pole-saliency (refer to Fig. 7 in the folowing).
2) It can allow 250% rated torque at standstill, under which strong flux saturation usually occurs.
3) It can allow ultralow speed control. The observed minimum speed ratio to the rated speed under the rated motoring or regenerating load is 1/1800.
4) In spite of the ultralow speed performance, it can operate up to the rated speed.
5) It can allow instant injection of the rated load even for zero-speed control.
6) It can allow accommodation of a load with huge moment of inertia.
7) It is insensitive to all of motor parameters such as stator resistance, stator inductance and rotor magnet flux.
8) It is also insensitive to saturation phenomena of stator flux.
9) It is so simple that it can be implemented with no additional hardware.

In the zero-to-low speed range, the high frequency voltage generator (HFV) in Fig. 2 generates a rotational high frequency voltage command such as

$$\boldsymbol{v}_{1h}^* = V_{1h}\begin{bmatrix}\cos\omega_h t\\ \sin\omega_h t\end{bmatrix}, \tag{20}$$

ISSN 2032-6653

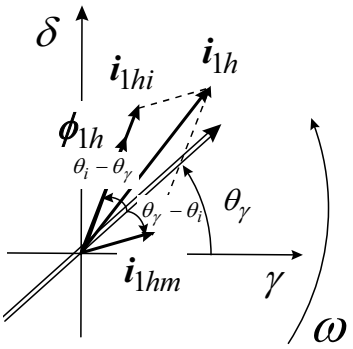

Fig. 7. Relation among phases of rotor-N-pole, in-phase current and mirror-phase current.

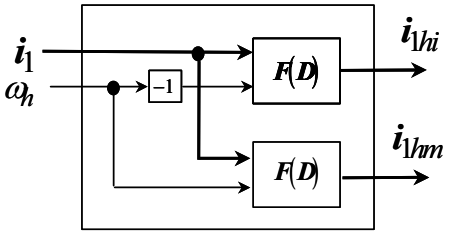

Fig. 8. Configuration of the in-phase mirror-phase current evolver based on filters in the D-module.

which is superimposed on the fundamental voltage command to produce the final stator voltage command. The injection of the rotational high frequency voltage yields a rotational high frequency current $\boldsymbol{i}_{1h}$, which consists of high frequency in-phase current $\boldsymbol{i}_{1hi}$ and high frequency mirror-phase current $\boldsymbol{i}_{1hm}$. According to the "mirror-phase characteristics," the rotor phase locates right at the center of the in-phase and mirror-phase currents (refer to Fig. 7). Based on the mirror-phase characteristics, the rotor phase can be estimated using the in-phase and mirror-phase currents such as

$$\left.\begin{aligned} \begin{bmatrix} C_{2p} \\ S_{2p} \end{bmatrix} &= [\boldsymbol{i}_{1hi} \quad \boldsymbol{J}\boldsymbol{i}_{1hi}]\boldsymbol{i}_{1hm} \\ \hat{\theta}_\gamma &= \frac{1}{2}\tan^{-1}\left(\frac{S_{2p}}{C_{2p}}\right) \end{aligned}\right\}, \tag{21}$$

where C_{2p}, S_{2p} of the first equation in (21) are the first and second elements of the 2x1 vector in the right hand side.

The lower blocks of the phase estimator in Fig. 4 performs phase estimation based on the mirror-phase estimation method. The "in-phase mirror-phase current evolver" extracts the in-phase and mirror-phase currents from the stator current, using information of a constant frequency ω_h of the high frequency voltage command. As shown in Fig. 8, the in-phase mirror-phase current evolver is constructed by means of the "filters in the D-module," which was originally proposed by one of the authors [10]. It is known that the filter in the D-module is robust to distortion of sinusoidal input signal, i.e. it produces almost pure sinusoidal output even for distorted input. This feature provides the phase estimation method using the filter in the D-module with robust to signal distortion caused by flux saturation and so on. The phase-error detector in Fig. 4 produces an initial phase estimate $\hat{\theta}_\gamma$ from the in-phase and mirror-phase currents. While the lower blocks of the phase estimator in Fig. 4 performs, the "switch" is in principle turned to L-side.

The phase estimator, which produces estimates of the rotor phase and speed instead of position sensors, makes sensorless drives possible, but does not energy-efficient and wide speed-range drives. It is made possible by the command generator and the command converter in Fig. 2.

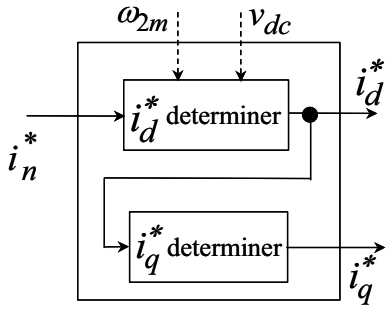

Fig.9. Basic configuration of the command converter

5. CONFIGURATIONS OF COMMAND GENERATOR AND COMMAND CONVERTER

5.1 Configuration of command generator

The proposed drive control system produces a signed current-norm command i_n^* from directions by the d-n-r hand lever and the acceleration foot pedal at the command generator in Fig. 2. The d-n-r hand lever directs drive modes such as d (drive), n (neutral), and r (reverse), and the foot pedal does the magnitude of the current-norm command, i.e.

$$i_n^* = \begin{cases} +\left|i_n^*\right| ; \text{ drive} \\ 0 ; \quad \text{neutral} \\ -\left|i_n^*\right| ; \text{ reverse} \end{cases} \tag{22}$$

where superscript * indicates commands. For the neutral direction, the signed current command is forced to be zero.

5.2 Configuration of command

The command converter produces d-, q-current commands i_d^*, i_q^* from a signed current norm command i_n^* so that an energy-efficient and wide speed-range drive can be attained with constraints as

$$\left.\begin{aligned} i_n^{*2} &= i_d^{*2} + i_q^{*2} \\ \text{sgn}(i_n^*) &= \text{sgn}(i_q^*) \end{aligned}\right\}, \tag{23}$$

where "sgn" means a sign-function whose output is a positive or negative unity [11]. Fig. 9 shows the internal structure of the command converter, which firstly determine analytically a d-current command from a signed current-norm command according to specific strategies, if necessary using rotor speed and dc-link voltage information

ISSN 2032-6653

as well, secondly does a q-current command simply based on (23). Note that d-, q-current commands are determined analytically with no necessity of approximation or recursive computation. The detailed explanations of the command converter are given in the following.

One of energy-efficient strategies in the constant torque region where no effective voltage limit exists is the one that maximizes ratio of torque per stator current-norm in order to minimize the copper loss due to the stator resistance. The optimal d-, q-current commands for the strategy commands are analytically obtained as [11]

$$\left.\begin{aligned} i_d^* &= \frac{-1}{2}\left(\frac{\Phi}{4L_m} + \sqrt{\frac{\Phi^2}{16L_m^2} + 2i_n^{*2}}\right) \\ i_q^* &= \mathrm{sgn}(i_n^*)\sqrt{i_n^{*2} - i_d^{*2}} \end{aligned}\right\}. \tag{24}$$

The most important factor to be considered in drive over the rated speed is the voltage limit. With no consideration of the voltage limit, high-speed drive in the overrating region cannot be attained. The optimal d-, q-current commands is analytically obtained as [11]

$$\left.\begin{aligned} i_d^* &= \frac{1}{4L_iL_m}(\alpha_3 + \beta_3) \\ \alpha_3 &= -\Phi L_d \\ \beta_3 &= \sqrt{\Phi^2 L_q^2 - 4L_iL_m\left(L_q^2 i_n^{*2} - \left(\frac{c_v}{\omega_{2n}}\right)^2\right)} \\ i_q^* &= \mathrm{sgn}(i_n^*)\sqrt{i_n^{*2} - i_d^{*2}} \end{aligned}\right\}. \tag{25}$$

The parameter c_v in (25) indicates a voltage limit in sense of norm of voltage vector. In the ideal case that inverters have no dead time, the voltage limit c_v turns out to be $v_{dc}/\sqrt{3}$, where v_{dc} is the dc-link voltage of inverters. In the case that inverters have a dead time of t_d and switching frequency is f_c, c_v is reduced to

$$c_v = \frac{v_{dc}}{\sqrt{3}}(1 - t_d f_c). \tag{26}$$

It is worthy of noting that the state stator current corresponding to (25) is optimal in the sense that it produces the maximum torque with the minimum copper loss under the voltage limit c_v.

In order that the analytical solution has physical meaning or is practical, the following constraints should be satisfied [11]

$$\left|\Phi - L_d\left|i_n^*\right|\right| < \left|\frac{c_v}{\hat{\omega}_{2n}}\right| < \sqrt{\Phi^2 + L_q^2 i_n^{*2}}\ . \tag{27}$$

Using motor parameters in Table 1, Fig. 10 shows a region as region B, where (27) gives a physically meaningful and/or practical solution. The upper hem curve of region B is governed by the right hand side of (27), and the lower hem straight lines by the left hand side. Region B clearly shows that the achievable maximum speed varies dependently on both voltage limit and the current-norm command.

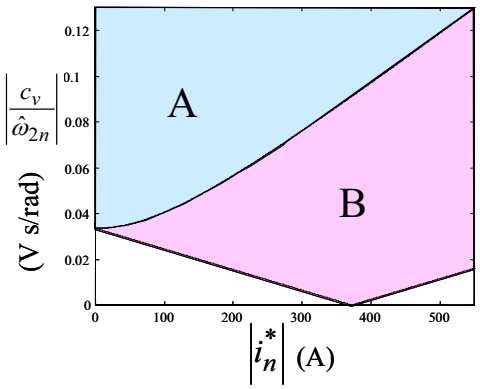

Fig. 10. Attainable operation region under voltage limit.

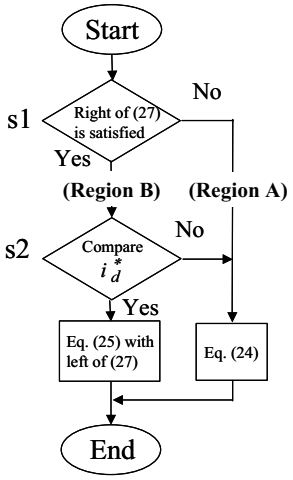

Fig. 11. Current command selection procedure.

Equation (27) yielding the unique analytical solution for maximum voltage strategy cannot be applied to Region A. However, this does not mean that region A is unusable. Region A corresponds to a driving case that rotor speed is too low. In other words, region A is the one where no consideration of voltage limit is necessary and pure energy-efficient strategy in (24) can be applied. Note that allowed total driving region includes both regions A and B, and that right hem of both regions A and B is governed by the allowed current norm.

Wide speed-range drives across regions A and B in Fig. 10 can be attained effectively by a combination of two strategies, one of which pursuits pure energy-efficiency under no effective voltage limit; the other does so but under effective voltage limit. Fig. 11 shows a flow chart that shows how two strategies are combined, in other words, is switched. At the first step, the inequality in right hand side of (27) is checked. If it is not satisfied, the optimal solution is located in region A in Fig. 10, and the solution by the maximum torque/current strategy i.e. (24) is selected. If satisfied, the optimal solution is located in region B. Even in region B, especially in neighborhood of the upper curve specified by right hand side of (27), there still exists possibility that the pure energy-efficient strategy can be selected. In order to examine the possibility, go to the second step, and compare two d-current commands by (24) and (25). According to the comparison, select the solution

ISSN 2032-6653

Fig. 12. Inverter for the ST-EV.

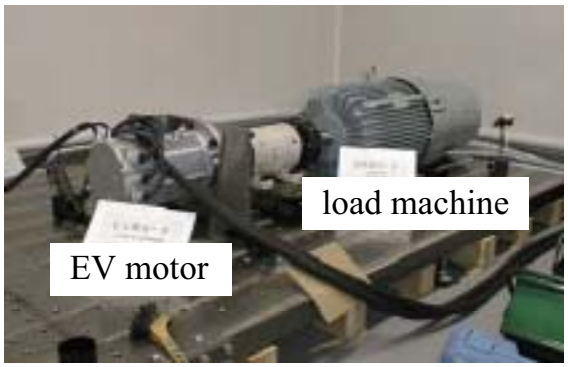

Fig. 13. SP-PMSM for ST-EV on test bed.

whose negative d-current command is less than the other.

The selecting function in Fig. 11 and the first equations in (24) and (25) are implemented in the i_d^* determiner of the command converter in Figs. 2 and 9. The i_q^* determiner of the command converter comprises the second equation in (24) and (25).

6. EXPERIMENTS

6.1 Experiments on test bed

Figs. 12 and 13 show a prototyped drive control apparatus corresponding to the dashed block in Fig. 2 and a SP-PMSM for a main EV traction motor coupled with a load machine on a test bed, respectively (refer to Table 1 for motor characteristics). The SP-PMSM was driven by the apparatus, which switches frequency-hybrid mode at electrical speed 600-rad/s (mechanical speed 150-rad/s). The high frequency voltage was selected as $V_{1h} = 2$ -V, $\omega_h = 800\pi$ -rad/s in experiments on the test-bed.

Fig. 14 is a response at the rated mechanical speed 400-rad/s to a signed current-norm command of i_n^* =233-A capable of producing the rated torque 40-Nm. At the speed, d- and q-current commands are determined based on (24) by the command converter in Fig. 9, the HFV is turned off, no high frequency voltage is superimposed, the "switch" in Fig. 4 is turned to H-side, and an initial phase estimate is determined by the D-state-observer. Fig 14 shows, from the top, q-current, d-current, actual rotor phase, and its final estimate. The average values of q-, d-currents are controlled to be equal to the associated commands, although they have

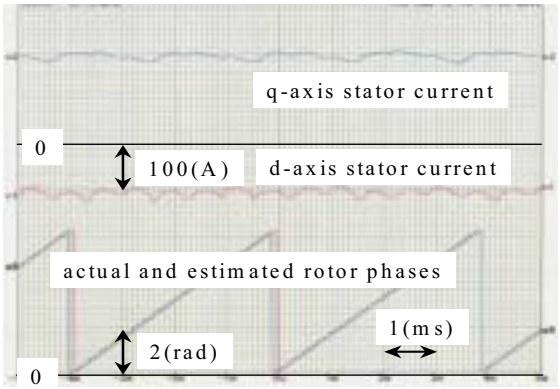

Fig. 14. A response of SP-PMSM producing rated 40-Nm torque at speed of 400-rad/s.

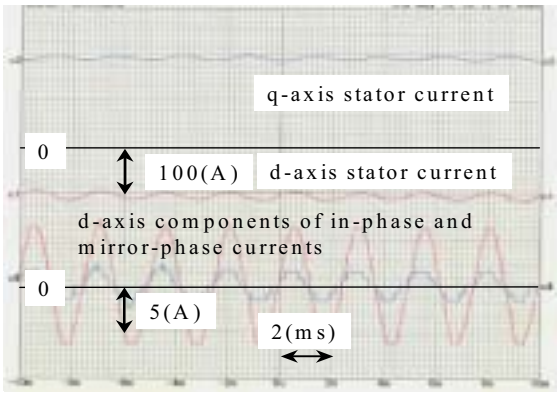

Fig. 15. A response of SP-PMSM producing rated 40-Nm torque at standstill.

some ripples. Rotor phase is smoothly estimated due to low-pass filtering effects by the D-state-observer. The estimation error to actual phase is about ± 0.1-rad under the rated load.

Fig. 15 is a response at standstill where signed current-norm, d-current, and q-current commands are the same as in Fig. 14. However, HFV is turned on, and a high frequency voltage command is superimposed on the fundamental voltage command, the "switch" in Fig. 4 is turned to L-side, and an initial phase estimate is determined by the mirror-phase estimation method. Fig 15 shows, from the top, q-current, d-current, d-components of high frequency in-phase and mirror-phase currents $\boldsymbol{i}_{1hi}$, $\boldsymbol{i}_{1hm}$. The ripples on d- and q-currents correspond to the high frequency components, which are filtered out as in-phase and mirror-phase currents. No phase difference between the d-components of the in-phase and mirror-phase currents means that rotor phase is well estimated. The maximum estimation error to actual phase is about ± 0.2-rad under the rated load, and the average error is nearly zero.

6.2 Experiments by prototype EV

The prototyped drive control apparatus was installed in a ST-EV as well as the traction motor. Fig. 16 shows an appearance of the apparatus mounted on the rear of the ST-EV. Experiments using the ST-EV were carried out on a chassis dynamometer as shown in Fig. 17. Experimental data such as U-phase current, dc-bus voltage, which are accessible from outside of the apparatus, were taken.

ISSN 2032-6653

Fig. 16. Developed drive-control apparatus mounted on ST-EV.

Fig. 17. ST-EV on chassis dynamometer.

Fig. 18 shows a response at drive speed about 50-km/h (about mechanical rotor speed of 600-rad/s). It indicates, from the top, dc-bus voltage and U-phase current. The stator current is well controlled as observed. At this speed, the HFV is turned off, no high frequency voltage is superimposed, the "switch" in Fig. 4 is turned to H-side, and an initial phase estimate is determined by the D-state-observer.

Fig. 19 shows a response at drive speed about 5-km/h (about mechanical rotor speed of 60-rad/s). The meaning of the waveform data is the same as in Fig. 18. High frequency components of $\omega_h = 800\,\pi$ -rad/s due to a high frequency voltage command are clearly observed, i.e., at this speed, HFV is turned on, and a high frequency voltage command is superimposed on the fundamental voltage command, the "switch" in Fig. 4 is turned to L-side, and an initial phase estimate is determined by the mirror-phase estimation method. Note that the amplitude of the high frequency voltage command was reset to a larger value $V_{1h} = 10$ -V than in the test-bed experiments, in consideration of both robustness to disturbance from road and high frequency acoustic noise.

After the necessary experiments, public-road drive of the prototyped ST-EV was started, which was called as "Shin II" after ST-EV "Shin" using an induction motor. Fig. 20 is a picture of ST-EV Shin II driving in Yokohama Port area on March 25, 2004.

7. CONCLUSIONS

One of the most important technologies for EVs is drive control one for main traction motors. This paper proposed a

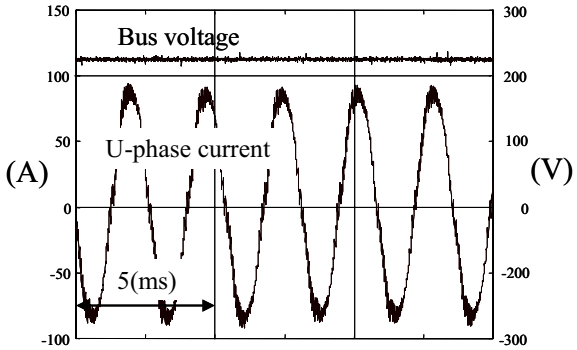

Fig. 18. A response example of driving of about 50-km/h.

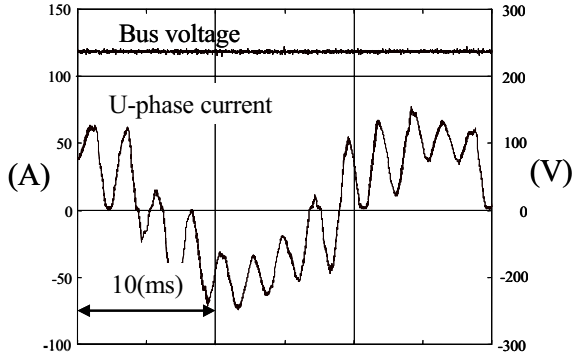

Fig. 19. A response example of driving of about 5-km/h.

Fig. 20. The ST-EV driving on public road of Yokohama Port area on March 25, 2004.

new sensorless drive control system that allows realization of ST-EVs using a permanent-magnet synchronous motor as a main traction motor. The proposed drive control system has the following potential characteristics: 1) it is based on vector control methods that allow quick, efficient and/or precise torque production; 2) it does not require a position/speed sensor for controlling motor drive, which has been mounted on a rotor shaft; 3) it can produce high torque even at standstill and can have wide driving-range, consequently can allow development of ST-EVs. Potential usefulness of the proposed drive control system was examined through the development of a prototype ST-EV capable of driving on public road.

ISSN 2032-6653

REFERENCES

[1] M. Schroedl, D. Hennerbichler, and T. M. Wolbank: "Induction Motor Drive for Electric Vehicles without Speed and Position Sensors", Proc. of 5-th European Conference on Power Electronics and Application (EPE-93), pp.271-367, 1993.

[2] S. Shinnaka and S. Takeuchi: "Development of a Radical New Sensorless-Vector-Controlled and Transmissionless Electric Vehicle", Proc. of 19th International Battery, Hybrid and Fuel Cell Electric Vehicle Symposium and Exhibition (EVS 19), pp.1467-1478, 2002

[3] N. Patel, T. O'Meara, J. Nagashima, and R. Lorenz: "Encoderless IPM Drive System for EV/HEV Propulsion Applications", CD-Proc. of 9-th European Conference on Power Electronics and Application (EPE 2001), 2001.

[4] N. Patel, T. O'Meara, J. Nagashima, and R. Lorenz: "Encoderless IPM Drive System for EV/HEVs", CD-Conference Record of the 2001 IEEE Industrial Applications Conference (36th IAS Annual Meeting, IAS-2001), 2001.

[5] R. Masaki, S. Kaneko, M. Hombu, T. Sawada, and S. Yoshihara: "Development of a Position Sensorless Control System on an Electric Vehicle Driven by a Permanent Magnet Synchronous Motor", Proc. of Power Conversion Conference-Osaka (PCC-Osaka 2002), pp.571-576, 2002.

[6] S. Shinnaka: "Frequency-Hybrid Vector Control with MIR Strategy for Sensorless Synchronous Motor Drive", Proc. of 31st Annual IEEE Power Electronics Specialists Conference (PESC 2000), Vol.1, pp. 442-447, 2000.

[7] C.Silva, G. M. Asher, and M. Sumner: "Hybrid Rotor Position Observer for Wide Speed-Range Sensorless PM Motor Drives Including Zero Speed", IEEE Trans. Industry Electronics, Vol.53, No. 2, pp.373-378, 2006.

[8] S.Shinnaka: "New D-State-Observer-Based Vector Control for Sensorless Drive of Permanent-Magnet Synchronous Motors", IEEE Trans. Industry Applications Vol.41, No.3, pp.825-833, 2005.

[9] S. Shinnaka: "New Mirror-Phase Vector Control for Sensorless Drive of Permanent-Magnet Synchronous Motor with Pole Saliency", IEEE Trans. Industry Applications Vol. 40, No.2, pp.599-606, 2004.

[10] S. Shinnaka: "A New Characteristics-Variable Two-Input/ Output Filter in the D-Module, -- Designs, Realizations, and Equivalence--", IEEE Trans. Industry Applications Vol.38, No.5, pp.1290-1296, 2002.

[11] S. Shinnaka: "A New Norm-Based Current Control Method for Energy-Efficient/Wide-Speed-Range Drive of Salient-Pole Permanent-Magnet Synchronous Motors", Proc. of 37th Annual IEEE Power Electronics Specialists Conference (PESC 06), pp.1340-1346, 2006.

BIOGRAPHIES

Shinji Shinnaka graduated from the National Defense Academy, Yokosuka, Japan in 1973, received the M.S. and Ph.D. degrees from the University of California, Irvine, USA in 1977 and 1979, respectively, and received the Dr.Eng. degree from Tokyo Institute of Technology, Tokyo, Japan in 1990. After serving in the First Research Institute, Japan Defense Agency, and the Department of Electrical Engineering, the National Defense Academy, he was with Canon Inc., as the Head of several research laboratories, from 1986 to1991. He established a venture research company in the Tokyo area in 1991 and acted as its President. Since 1996, he has been a Professor in the Department of Electrical Engineering, Kanagawa University, Yokohama, Japan. He has worked in a wide range of fields including communication, information, control engineering, and power electronics, as a researcher, engineer, educator, and director. He developed the first sensorless-vector-controlled electrical vehicles with no variable transmission, one of which uses an induction motor, and the other uses a permanent-magnet synchronous motor.

Prof. Shinnaka has received Best Paper, Best Book, and Best Technology Awards from the Society of Instrument and Control Engineers, Japan, and a Prize Paper Award from the IEEE TRANSACTIONS on INDUSTRY APPLICATIONS.

Shigeru Takeuchi received B.Eng. degree from Kanagawa University, Yokohama, Japan in 1978. Since 1977, he has been a technician in the Department of Electrical Engineering, Kanagawa University. He developed the first sensorless-vector-controlled EVs with no variable transmission, one of which uses an induction motor, another a permanent-magnet synchronous motor, together with Prof. Shinnaka.